





Article

Proposed Solution for Stony Debris-Flow Control Works in Two Headwater Basins with Morphological Changes

Mauro Boreggio [†], Matteo Barbini [†], Martino Bernard [†], Massimo Degetto  and Carlo Gregoretti ^{*}

Department Land, Environment, Agriculture and Forestry, University of Padova, 35020 Legnaro, PD, Italy; mauro.boreggio@unipd.it (M.B.); matteo.barbini@unipd.it (M.B.); martino.bernard@unipd.it (M.B.); massimo.degetto@gmail.com (M.D.)

* Correspondence: carlo.gregoretti@unipd.it

[†] These authors contributed equally to this work.

Abstract: Stony debris flows originating from the two basins of Jaron di Sacomedan and Jaron dei Ross pose a significant threat to the inhabited area of Chiapuzza (Dolomites, Northeastern Italian Alps) and the national road SS 51. In the upper part of the Jaron dei Ross basin, a large scree at the foot of a rocky amphitheater undergoes morphological changes due to frequent rockfalls. Previous mitigation efforts have proven inadequate, and after identifying the causes of their failure, new control measures are being planned. These works aim to direct debris flows towards a deposition area capable of intercepting flows from both the Jaron dei Ross and Jaron di Sacomedan basins. Essentially, the upper works in the Jaron dei Ross basin divert debris flows away from the populated area and channel them to a location where the sediment volume transported by debris flows from both basins can be stored. This solution is designed to protect both the Chiapuzza community and the SS51 national road.

Keywords: stony debris flow; control work; flow diversion and guidance; deposition area



Citation: Boreggio, M.; Barbini, M.; Bernard, M.; Degetto, M.; Gregoretti, C. Proposed Solution for Stony Debris-Flow Control Works in Two Headwater Basins with Morphological Changes. *GeoHazards* **2024**, *5*, 1346–1369. <https://doi.org/10.3390/geohazards5040064>

Academic Editor: Kevin Schmidt

Received: 8 August 2024

Revised: 3 December 2024

Accepted: 4 December 2024

Published: 18 December 2024



Copyright: © 2024 by the authors. Licensee MDPI, Basel, Switzerland. This article is an open access article distributed under the terms and conditions of the Creative Commons Attribution (CC BY) license (<https://creativecommons.org/licenses/by/4.0/>).

1. Introduction

Stony debris flows, which are mixtures of gravel, sand, and water with a small percentage of lime and clay that move downstream at high speed along steep slopes, are the most common hazard in the Dolomitic area [1,2]. They are generated by the impact of abundant runoff delivered by rocky cliffs after high-intensity rainfalls against debris material [3–6]. The impact of runoff against the debris material leads to the formation of a solid-liquid surge followed by a fluid body that increases its volume up to ten times due to the entrainment of solid material [7–9]. The volumetric growth usually occurs in the high-sloping reach of the debris-flow (DF) channels [10], where bed-slope angles are larger than 20° [11]. The intermediate-sloping and low-sloping reaches of the debris channels are dominated by transport (a near balance between erosion and deposition) and deposition, respectively. The increasing frequency of debris-flow events due to the rise in extreme rainfalls providing abundant runoff [12,13] and cliff or slope-failure events providing debris material [14–16], along with their destructive power due to the large volumes of transported sediment, calls for structural countermeasures to protect inhabited areas and transport infrastructures [17–19]. Most control works focus on detaining the sediment volume transported by debris flows, using retention basins [20,21] and deposition areas [22,23] or a combination of both [24]. These works are placed along the routing path of debris flows to intercept and store the sediment. In cases where the terrain geomorphology does not allow for excavation and building such works to store the sediment is not possible, the flow path should be directed to areas where this is feasible. Flow guiding usually presents no difficulties in the middle and lower parts of a basin [25], except in the upper part, which may have a complex geomorphology.

In this work, we introduce an approach for guiding debris flows along a path different from the natural one when the site is subject to morphological changes. The approach is applied in the Jaron dei Ross headwater basin, where a debris-flow channel that incises a scree directly points to the inhabited area of Chiapuzza (municipality of San Vito di Cadore) in the Dolomites (Northeastern Italian Alps). The scree is beneath a rocky cliff that is frequently subjected to failures, and the fallen material continuously changes its morphology. Previous works to deviate the debris-flow channel failed. Here, using geophysical methods for the first time in a scree, we show the reasons for the failures of previous works and propose a new solution. The guidance works drive the debris flows to a deposition area that also stores the sediment volume arriving from the neighboring basin of the Sacomedan headwater basin.

The paper is organized as follows: Section 2 discusses the materials and methods, covering the study site, previous works, the procedure for determining the design solid-liquid hydrographs, including the models for simulating runoff and debris-flow routing, as well as the method for sizing a deposition area. Section 3 presents the approach for driving the debris flow to works where the sediment volume can be stored. Section 4 discusses the results of the proposed approach in the case study. Finally, Section 5 discusses the conclusions.

2. Materials and Methods

2.1. The Chiapuzza Site

A reach of the national road and the inhabited area of Chiapuzza, located just below it in the Dolomites (Northeastern Italian Alps), is threatened by debris flows originating from the Jaron di Sacomedan and Jaron dei Ross headwater basins (Figure 1). Two debris-flow channels incise the scree at the base of rocky cliffs and, separately, point downstream along nearly the maximum inclination direction. Both the debris-flow channels run alongside a rocky cliff on the left side. In the Jaron di Sacomedan basin, the lateral cliff ends just upstream of the fan apex, whereas in the Jaron dei Ross basin, it ends well downstream of the fan apex. Therefore, in the latter case, it is not possible to build a retention basin for the storage of sediment volume due to the limited space available between the end of the cliff and the national road.

In 1966, a debris flow routed along the channel on the Jaron dei Ross scree (Figure 2) impacted the national road and inundated the inhabited area of Chiapuzza. A channel (DF channel 5 in Figure 2) was built, but due to its wide attack angle, it failed to convey the subsequent debris-flow event in 1970, which again impacted the national road and inundated Chiapuzza. Therefore, in the 1970s and 1980s, the debris-flow channel originating on the scree of the Jaron dei Ross basin was blocked by means of a wall, and the debris flow was redirected along DF channel 1 (Figure 2) towards the channel descending from the Jaron di Sacomedan basin. The two channels joined downstream in a small deposition area. Another channel linked the deposition area to a retention basin just upstream of the national road SS 51. Between 1980 and 2010, the wall was subjected to piping and was subsequently rebuilt. The latest wall (Figure 3) in 2013 had most of its foundations uncovered (Figure A1) and partially failed during the Vaia storm in 2018 [26]. After a large rockfall occurred on 9 October 2021, the remaining part of the wall was completely wiped out, and the old Jaron dei Ross debris-flow channel was restored. In July 2013, two numeral and five volumetric samples were taken from DF channel 1 according to [27]. The results of the grain-size analysis are shown in Figure 4. The average values of d_{16} , d_{50} , d_{84} , and d_M for the volumetric samples are 0.0004 m, 0.0024 m, 0.105 m and 0.03 m, respectively, whereas those for the numeral samples are: 0.018 m, 0.046 m, 0.189 m, and 0.09 m. In addition, using the volumetric samples, the dry bed volumetric concentration was measured, yielding an average value of $c_* = 0.73$ (porosity 27%). Part of the volumetric sample was also used for the triaxial shear test (TxCID) within a cylinder 0.208 m high and with a diameter of 0.1 m, which was carried out in the Geotechnical Engineering Laboratory of the Department of Civil, Environmental and Architectural Engineering at the Padova University. The results

indicated a peak friction angle of 44.1° and an ultimate friction angle of 39° . Regarding the Sacomedan basin, a numeral sample provided the following values for the characteristic diameters: $d_{16} = 0.012$ m, $d_{50} = 0.034$ m, $d_{84} = 0.145$ m, and $d_M = 0.06$ m.

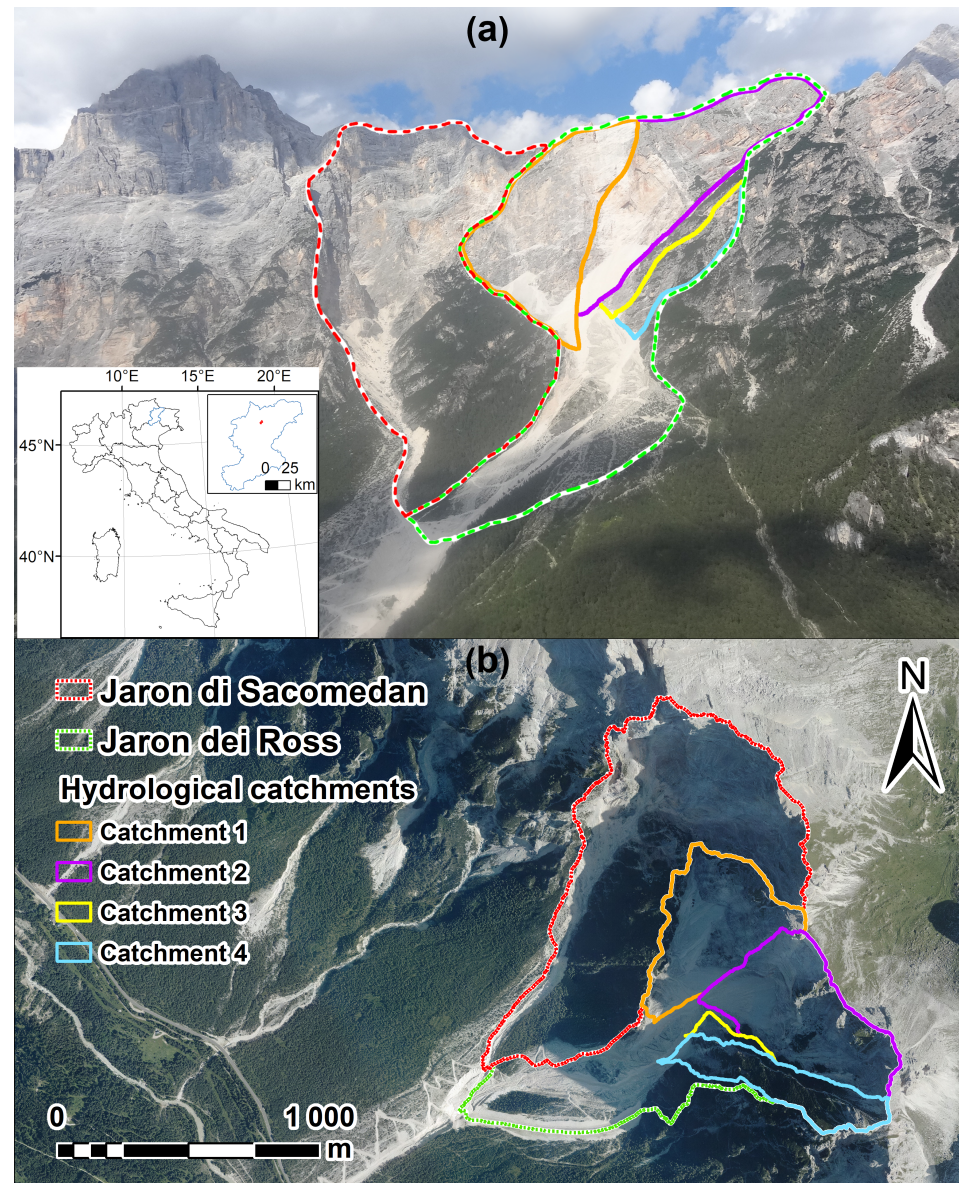


Figure 1. Frontal (a) and plan (b) views of the Sacomedan and Jaron dei Ross basins with the hydrological Catchments (1–4) that contribute to debris-flow occurrences.

The causes of wall piping were investigated using electrical tomography, which was conducted on the upper part of the scree in the Jaron dei Ross basin on June 2013, between the base of the cliffs and about 20 m downstream of the wall (Figures 5 and 6a). The lines ERT1-3 and ERT4-6 of Figure 6b were 850 m and 290 m long, respectively, with the electrodes placed at intervals of 3 m and an investigation depth of up to 15 m. The lines ERT7-8 had an investigation depth up to 30 m. The resistivity data obtained using a SAS 1000 georesistivimeter manufactured by ABEM company (Sweden) were transformed into terrain typology (bedrock, debris deposit, areas with ice or water). The profiles of the terrain typology were imported into a GIS for the creation of a digital elevation model of the bedrock, with its contour lines shown in Figure 6b. These contour lines reveal the main drainage paths of subsurface flow, indicating that the wall is located at a convergence point of subsurface flow for more than half of the upper part of the scree in the Jaron dei

Ross basin. The most probable locations for subsurface drainage pathways reside where permeable sediments are carved within the scree, lying over the bedrock. This is the most favorable thermodynamic configuration from subsurface flow systems [28].

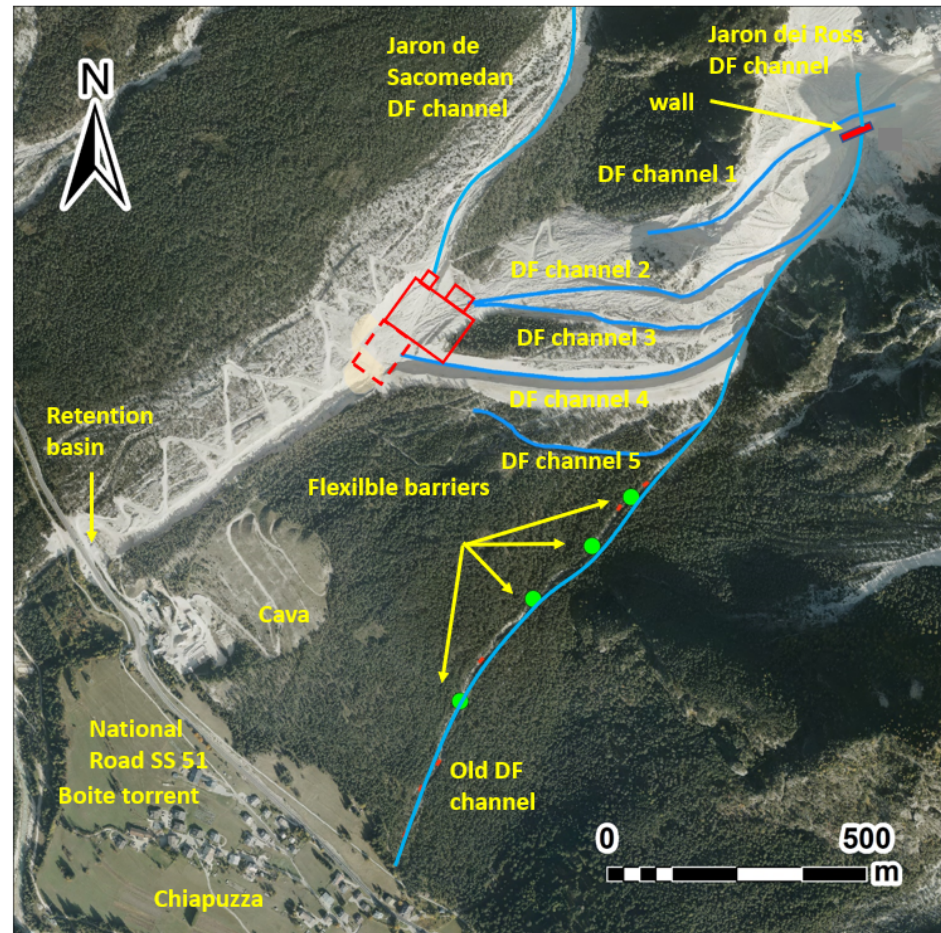


Figure 2. Plan view of the lower part of the Jaron di Sacomedan and Jaron dei Ross basins showing the control works, including DF channels 1–5, the wall, the old deposition area (red dotted line), and the new extension of the deposition area (red continuous line).

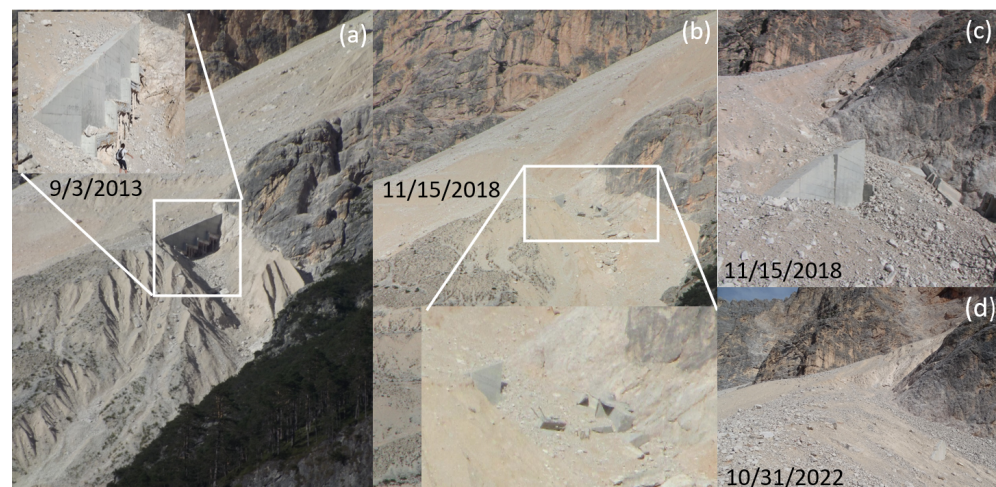


Figure 3. Downstream view of the wall and the upper part of the Jaron dei Ross debris-flow channel in 2013 (a) and after the VAIA storm in 2018 (b). Panels (c,d) show lateral views of the wall after the Vaia storm in 2018 and the rock failure in 2021, respectively.

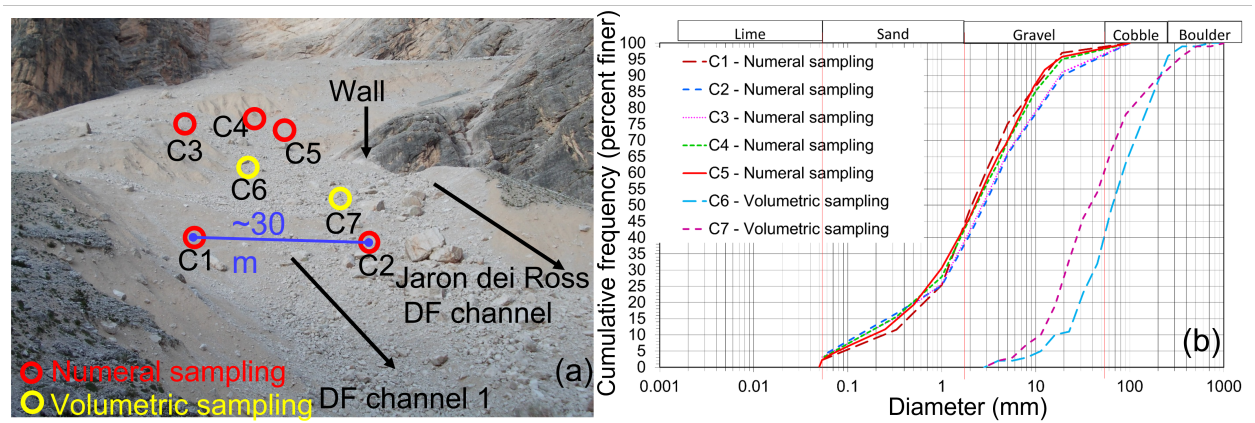


Figure 4. Sampling area on DF channel 1 just upstream of the wall (a) and the grain-size analysis of all the samples (b).

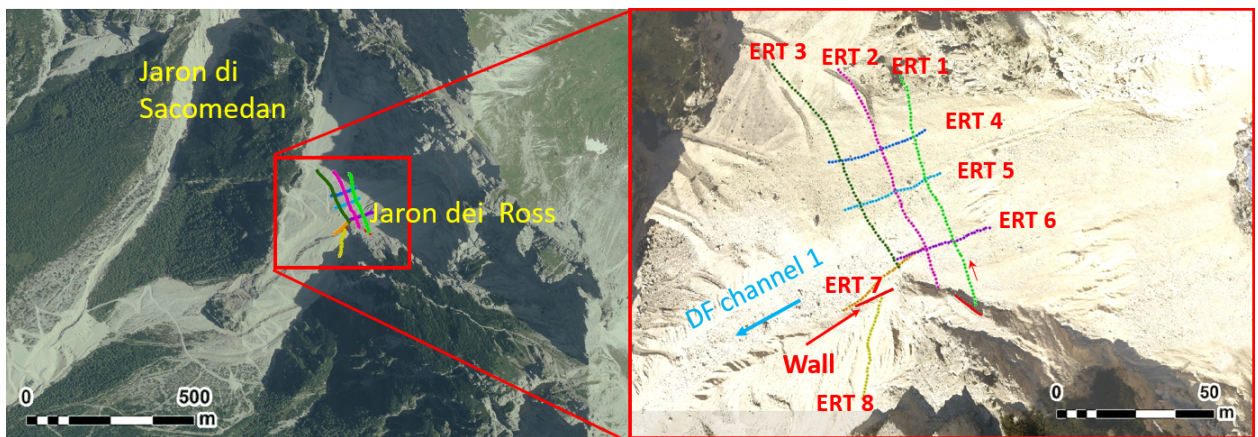


Figure 5. Aerial map of the two basins, showing the lines on the scree of the Jaron dei Ross basin where the electrical tomography was carried out.

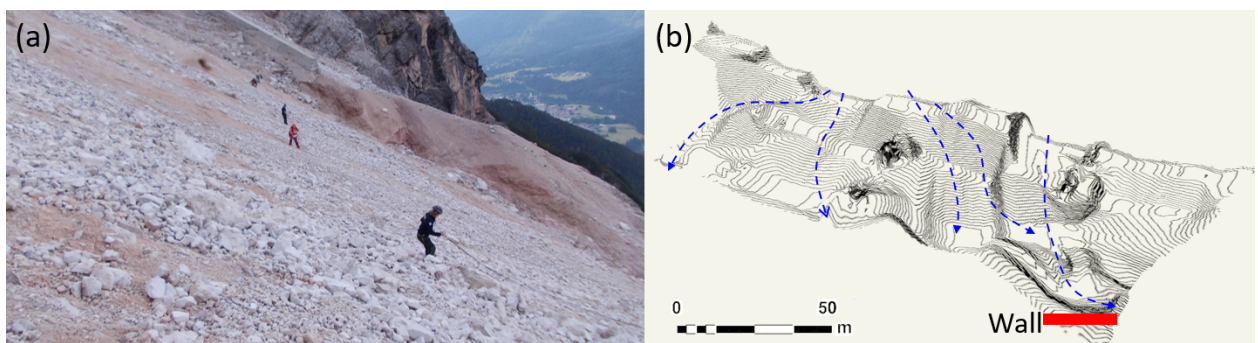


Figure 6. The electrical tomography on the upper part of the scree below the cliffs in the Jaron dei Ross basin (a) and the resulting contour lines of the bedrock with the main drainage lines (b) (blue arrows).

An analysis of the aerial photographs further shows that the debris-flow channel originating at the base of the cliffs is ephemeral: such a channel forms because of the excavation caused by runoff delivered by cliffs in some points of the scree, and it is frequently covered by debris material from rock failures of the overhanging cliffs. Figure 7 shows the upper part of the scree in 2013, 2018, and 2021. In 2013, there was no channel originating at the base of the cliffs (Figure 7a), whereas, in 2018, there are two channels starting from the base of the cliffs and incising the scree (Figure 7b,c). By 2021, after a

rock failure, one channel was missing (the one on the right), and the other was partially covered by debris material (Figure 7d). This is also clearly visible from the shaded DEM (Figure 7d,f). The upper part of the Jaron di Sacomedan channel runs over bedrock, with a rocky cliff bordering the left side, and is covered by giant boulders (Figure 8a). The presence of these giant boulders and the stabilizing effect of the bedrock on the slope on the right side limit the debris supply. At the end of the bedrock and lateral rocky cliff, the channel becomes highly erodible and significantly enlarges (Figure 8b). Figure A2 shows the enlargement and deepening of the channel in recent years. The limited supply of debris material upstream of the enlargement causes the flow in the upper part of the Sacomedan channel to develop into a hyperconcentrated flow.

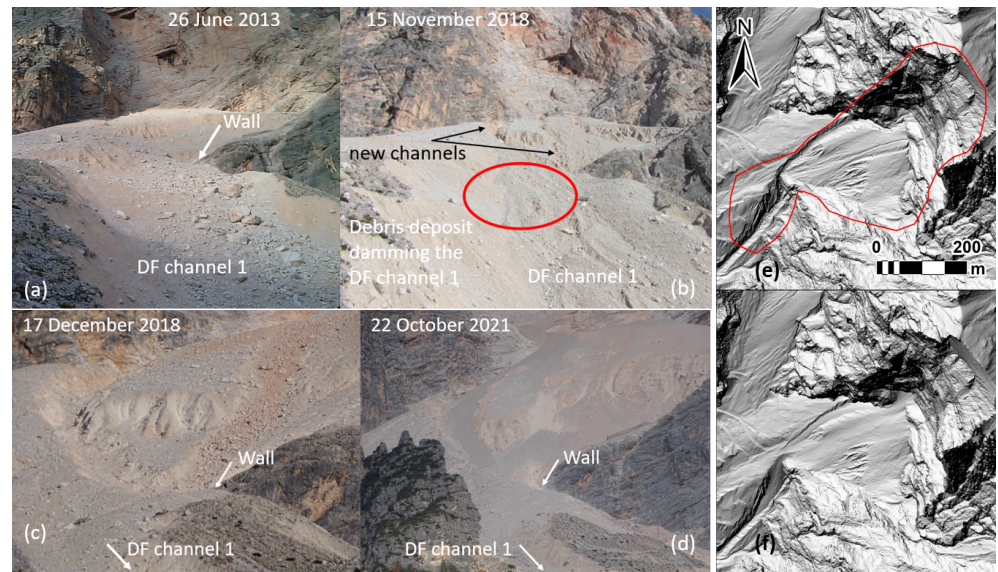


Figure 7. Frontal view of the upper part of the Jaron dei Ross scree in 2013 (a) and 2018 (b). Panels (c,d) show details from 2018 and 2021, respectively, while (e,f) display the corresponding shaded DEMs. The red line in panel (e) indicates the border of the area hit by the rock failure in 2021.

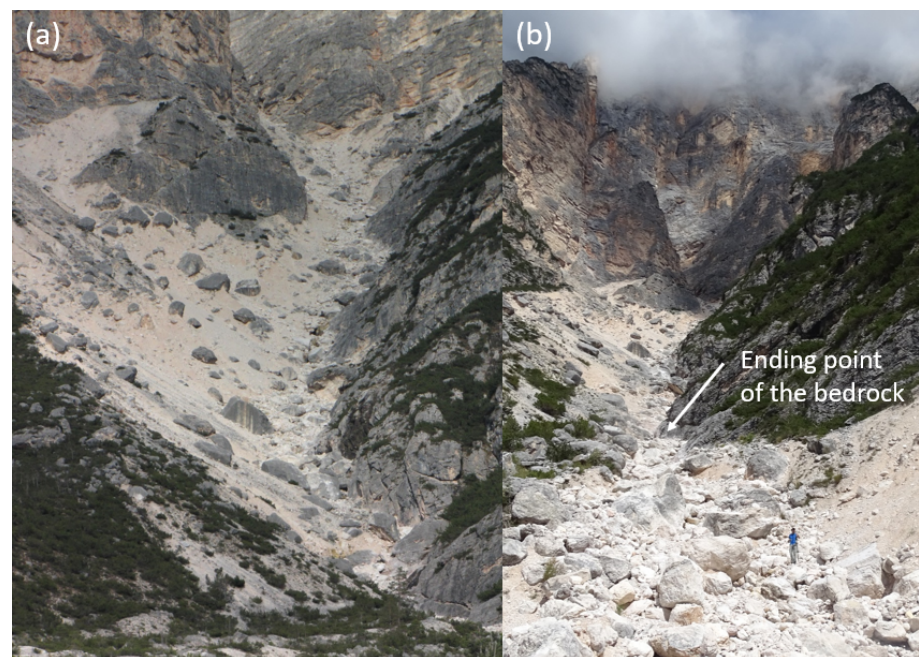


Figure 8. Frontal views of the upper (a) and lower (b) parts of the Jaron di Sacomedan basin.

2.2. The Hydrological Model

The event-based rainfall-runoff model developed by [29] simulates the runoff generated by rocky cliffs. The model essentially simulates both infiltration excess and interflow contributions for each pixel of the basin and routes these contributions along the steepest flow path to the channel network. It uses constant land-use-specific slope velocities. The first contribution, $i - f_c$, occurs when the rainfall intensity, i , exceeds the infiltration rate f_c . This is computed using a simplified Horton equation with a constant infiltration rate. The second contribution becomes active when $i < f_c$ and is computed using the Curve Number method of the Soil Conservation Service (SCS-CN). Runoff along the channel network is propagated to the catchment outlet using the matched diffusivity kinematic model of [30]. The model parameters include the curve number CN , the infiltration rate f_c , the slope velocity U_S , and the Gauckler-Strickler coefficient K_S . The values of the parameters, obtained by calibrating the model against discharges measured at the outlet of a rocky channel in Fiames (municipality of Cortina d'Ampezzo), are shown in Table 1. The only changing parameter for rocky terrains is the infiltration rate, which linearly depends on the 5-minutes maximum intensity recorded during the rainfall event [31]. This model effectively reproduces the peaky hydrological response observed at the base of rocky cliffs in the Dolomitic area.

Table 1. Calibrated parameters of the rainfall-runoff model updated by [31]. The relation for evaluating the Hortonian infiltration f_c (cm/hr) considers the 5-minutes maximum intensity I_{MAX5} recorded during the considered rainfall event (expressed in mm/hr).

Parameter	
CN	
Rocks	91.3
Scree	65
Bushes	61
U_S (m/s)	
Rocks	0.7
Other terrains	0.1
K_S ($m^{1/3}/s$)	9
f_c (cm/hr)	
Rocks	$0.090I_{MAX5} - 0.37$
Scree	10.5
Bushes	6.5

2.3. The Computation of Solid-Liquid Hydrographs

The solid-liquid hydrograph is significant in debris-flow risk management, as it provides the sediment volume necessary for planning and preliminary sizing of control works [24]. The shape of solid-liquid hydrographs can vary depending on the location where they are estimated and the scenario considered. In the case of a debris flow that has not yet been fully developed, the solid-liquid hydrograph is derived from the runoff hydrograph contributing to the debris flow, scaled by the ratio V_{SL}/V_{CR} . Here, V_{SL} represents the solid-liquid volume, and V_{CR} denotes the runoff volume contributing to the debris flow, that is, the volume of the runoff hydrograph that exceeds the threshold discharge required to trigger debris flow:

$$Q_{SL} = \frac{V_{SL}}{V_{CR}} Q \quad (1)$$

According to [24],

$$\frac{V_{SL}}{V_{CR}} = \frac{c_*}{c_* - c} \quad (2)$$

where c and c_* are the volumetric concentration of the flow and dry bed, respectively. Substituting the second member of Equation (2) in Equation (1), it yields

$$Q_{SL} = \frac{c_*}{c_* - c} Q \quad (3)$$

If the debris flow is fully developed with a well-defined front followed by a solid-liquid body, the solid-liquid hydrograph typically assumes a triangular shape. The peak discharge of this triangular hydrograph is given by the following relationship [32]:

$$\frac{Q_P}{Q_0} = 0.75 \frac{c_*}{c_* - c_F} \quad (4)$$

where Q_0 is the formative runoff peak discharge, and c_F is the solid-volumetric concentration of the solid-liquid front. The factor of 0.75 accounts for the contribution of the liquid discharge to the liquid queue of the debris flow. The value of c_F can be computed through the relationship proposed in [33] and updated in [32]:

$$c_F = \frac{\rho_f \tan \theta}{(\rho_s - \rho_f)(\tan \varphi_{qs} - \tan \theta)} \quad (5)$$

where ρ_f and ρ_s represent the densities of the liquid and solid phases, respectively; θ is the bed-slope angle; and φ_{qs} is the quasi-static friction angle. The rising limb of the triangular solid-liquid hydrograph is 1 min, and its duration is $2V_{SL}/Q_P$.

Another relationship for estimating c_F is provided in [34]. In cases of very high bed slopes, the relationships proposed in [32] and Lien and Tsai [34] may not be applicable. In such cases, c_F is assumed to be $0.9c_*$ according to [33]. The values of c have been provided in [24,35] and depend on the position and scenario. If the hydrographs are used for pre-sizing control measures, the value of c may need to be adjusted if the distance from the control works is significant. The surface threshold discharge for debris-flow triggering per unit width, q_{TR} , which is used to compute the runoff contributing to debris flow, can be determined using the relationship proposed by [36]:

$$q_{TR} = 0.78 \frac{d_M^{1.5}}{\tan \theta^{1.27}} \quad (6)$$

where θ is the bed-slope angle of the channel. The contributing runoff discharge is the simulated runoff discharge that exceeds the sum of the surface threshold discharge and the subsurface flow discharge. Such approach was also followed in [37,38].

2.4. The Routing Model

The model for simulating the routing of stony debris flows is the multi-processor version [24] of the model proposed in [39]. The model is raster-based and implements the kinematic approximation for the momentum equations of a bi-phase solid-liquid flow. There are five model parameters: the conductance coefficient, C , controlling the flow resistance, and the limit values of the bed-slope angle θ and flow velocity V , for which deposition and erosion can occur: $(\theta_{LIM-D}, U_{LIM-D})$ and entrainment $(\theta_{LIM-E}, U_{LIM-E})$. The conductance coefficient, C , is the ratio of the mean flow velocity to the shear stress, and it corresponds to a rheology dominated by collisions. The values of the parameters are those that well reproduce both the deposition-erosion pattern and the routing times of three high-magnitude occurred debris flows: $C = 5$, $\theta_{LIM-D} = 14^\circ$, $U_{LIM-D} = 1$ m/s, $\theta_{LIM-E} = 16^\circ$, and $U_{LIM-E} = 1.8$ m/s [20]. Ref. [20] carried out a sensitivity analysis and show that a change of the parameter values in a physically acceptable interval ($3 < C < 7$; $13^\circ < \theta_{LIM-D} < 15^\circ$; $14^\circ < \theta_{LIM-E} < 18^\circ$; $0.8 < U_{LIM-D} < 1.2$; $1.5 < U_{LIM-E} < 2.1$)

did not significantly vary the results of simulations. In the case of debris-flow of medium magnitude the conductance coefficient diminishes to 4 because according to the experiments of [32] and [40], the conductance coefficient increases with the peak discharge of runoff hydrograph that triggers the event. If the calibrated value of the conductance coefficient for high-magnitude debris flow is $C = 5$, that of a smaller-magnitude debris flow is lowered to $C = 4$, according to [24].

2.5. The Design Scenarios

According to Annex I of the *Flood Risk Management Plans* (European Flood Directive 2007/60/EC) of the Eastern Alps River Basin Authority, and also [24], there are two scenarios for debris-flow risk assessment: Maximum Peak Discharge (MPD) and Maximum Volume (MV), i.e., maximum solid-liquid discharge and volume, respectively. The MPD scenario is triggered by high-intensity, short-duration rainfalls, while the MV scenario is triggered by low-intensity, long-duration rainfalls. The duration of triggering rainfalls depends on the shape, size, and morphology of the basins and typically falls within the intervals of 10–30 min for MPD and 2–8 h for MV. The design rainfalls for these two scenarios are represented by different types of hyetographs: an alternating block hyetograph for MPD, which maximizes the peak runoff discharge and, thus, the solid-liquid peak discharge according to Equations (3) and (4), and a constant intensity hyetograph for MV, which maximizes the volume of contributing runoff to debris flows and, thus, the solid-liquid volume according to Equation (2). Detailed information about the triggering rainfalls can be found in [24]. In the MPD scenario, if the debris flow is in the initial stages of development, the solid-liquid hydrograph is the scaled hydrograph (Equation (3)); otherwise, if the debris flow is already fully developed, the hydrograph will be triangular. In the MV scenario, the solid-liquid hydrograph is always the scaled one due to the lower runoff discharge, which limits sediment entrainment and delays the development of a fully formed debris flow downstream.

Deposition Area: Scope, Use, and Sizing

Ref. [23] introduced the concept of a deposition area, which is a flat basin without embankment or berm on the downstream side, aimed at stopping or reducing the sediment volume transported by debris flows for small-medium and medium-high magnitude events, respectively. The authors of [23] provided a three-step procedure for designing a deposition area. The first step involves computing an initial or pre-sizing value of the area, A , and a horizontal projection of the bottom surface, using a simplified relationship between A and the design deposition volume, V_D :

$$A = \frac{V_D^{2/3}}{k_D} \quad (7)$$

where k_D is the dimensionless deposition coefficient, assumed to be 0.1. The second step is the design of the deposition area using this initial value. The third step involves computing the corresponding deposition volume as the sum of two components: (1) the volume between the sloping surface of angle φ_1 and the bottom surface of the deposition area, including the lateral banks, and (2) the volume between the sloping surface of angle φ_2 and the channel bottom and banks, as shown in Figure A3 of the Appendix B. The former volume, V_A , is computed as the difference between the prism V_V and the pyramids with bases A_{RB} and A_{LB} , with the height approximated by L . The latter volume is computed as the sum of the prism with height B_C and the pyramids of bases A_{CRB} and A_{CLB} . The relationship for computing V_D is

$$V_D = \frac{[B_D + B_U]L}{2}h_G - \frac{1}{3}(A_{RB} + A_{LB})L - \frac{1}{2}HhB_C + \frac{1}{6}H^2h(ctg\theta_{CRB} + ctg\theta_{CLB}) \quad (8)$$

where

$$\begin{aligned} H &= L \tan\varphi_1 \\ h &= H \frac{\cos\theta_C \cos\varphi_2}{\sin(\theta_C - \varphi_2)} \\ h_G &= L_G \tan\varphi_1 \\ L_G &= \frac{L}{3} \frac{B_D + 2B_U}{B_D + B_U} \\ A_{RB} &= 0.5B_{RB}^2 \tan\theta_{RB} \\ A_{LB} &= 0.5B_{LB}^2 \tan\theta_{LB} \end{aligned} \quad (9)$$

The quantities B_D and B_U represent the widths of the downstream and upstream edges of the deposition area, respectively. The quantities B_{RB} and B_{LB} are the right and left enlargements relative to the mouth of the incoming channel, respectively. The angles θ_{RB} and θ_{LB} are the slopes of the right and left banks of the deposition area, while B_C and θ_C are the width and bed-slope angle of the incoming channel, respectively. θ_{CRB} and θ_{CLB} denote the slopes of the right and left banks of the incoming channel, respectively. The values of φ_1 and φ_2 proposed in [16] are 15° and 6° , respectively. In scenarios with poor maintenance, where the deposition area is not emptied after small events, or in cases with two or more incoming channels, the value of φ_1 is reduced to 11° due to the presence of deposits, which causes preferential flow paths for new incoming flows, preventing homogeneous filling of the deposition area. In the presence of an upstream sloping part required for directing the flow along the longitudinal direction, Equation (8) changes. The details of these changes can be found in [23], which also provided a MATLAB[®] script for performing the calculation of the deposition area.

3. Results

The objective of the control works for the basins of Jaron di Sacomedan and Jaron dei Ross is to guide the flow to areas where sediment volume can be stored. In the first basin, the debris-flow channel is fixed, while in the second basin, the debris-flow channel must be diverted. The sizing of the works is based on solid-liquid hydrographs [24] because they provide an approximate value of the sediment volume that debris flows can transport.

3.1. Solid-Liquid Hydrographs

The catchments that provide the runoff triggering or contributing to debris flow include one for the Jaron di Sacomedan basin and four for the Jaron dei Ross basin (Figure 1). The hydrological basin of the Jaron di Sacomedan is closed where the bedrock and the rocky cliff on the left side end, and the channel becomes erodible and significantly enlarges (Figure 8b). Catchment 1 of the Jaron dei Ross basin collects all the runoff from the right side of the Jaron dei Ross, supplying the debris flows routing along DF channel 1 (Figure 2). Catchment 2 collects all the runoff and subsurface flow from the right side of the Jaron dei Ross basin, concentrating just upstream of the failed wall and initiating the debris flows. Catchments 3 and 4 consist of the cliff bordering the left side of the debris-flow channel of Jaron dei Ross and supply runoff to DF channels 2–3 (Figure 2). By using the same duration-frequency curve for the return period of 300 years as in [24] (due to the same rain gauge), the results of the hydrological simulations with the parameters shown in Table 1 are illustrated in Figure 9 for both scenarios. The rainfall used for the hydrological modeling derives from the rainfall depth frequency curve corresponding to the return period of 300 years according to the methodology introduced in [24]. The curve

is obtained using the Peak Over Threshold technique that considers all the values exceeding a threshold [41,42]. The use of the values exceeding a threshold allows for capturing an increase in the frequency of the extreme precipitations that determine the occurrence of debris-flow phenomena. Details on the definition of the threshold can be found in [24], while those on the POT technique are in Appendix A. Rainfall data used for determining the rainfall depth frequency curve are those of the of the Rovina Bassa rain gauge managed by ARPA (Regional Environment Protection Agency) [41]. The solid-liquid hydrographs are computed for the Jaron di Sacomedan basin and for Catchment 2, following the procedure outlined in Section 2.3. Both of the hydrographs are of the scaled type for two different reasons. In the first case, due to the limited supply of debris material, the debris flow cannot fully develop and remains a hyperconcentrated flow. In the second case, the outlet is close to the initiation area, so the debris flow is not yet fully developed. The bed-slope angles of the Jaron di Sacomedan channel (just upstream of the enlargement) and DF channel 1 (upstream of the failed wall) are 14.6° and 33° , respectively, while the widths are 7 and 6 m, respectively. By applying equation (6), the surface threshold discharge per unit width for the two basins is 0.064 and 0.046 m^2/s , respectively. The runoff threshold discharge is the sum of the surface threshold discharge and the subsurface discharge per unit width, q_{SUB} , estimated to be about 0.05 m^2/s according to the method proposed in [36]. The threshold discharges, $B(q_{TR} + 0.05)$, for the two basins are 0.796 and 0.576 m^3/s , respectively.

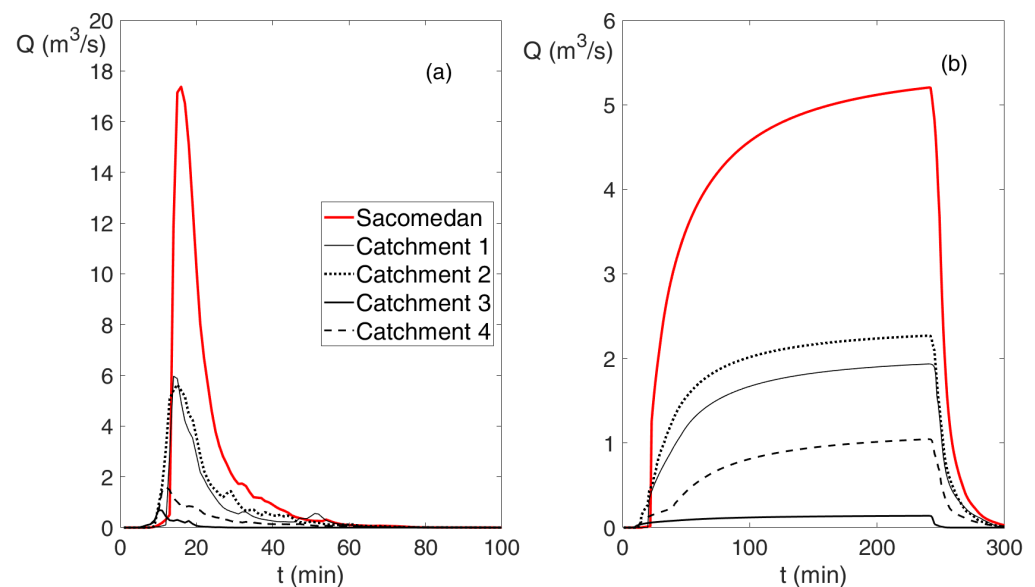


Figure 9. Simulated runoff hydrographs of the Jaron di Sacomedan basin and Catchments 1–4 of Jaron dei Ross basin corresponding to the MPD (a) and MV (b).

The solid-liquid hydrographs are used to compute the sediment volume necessary for sizing the deposition area. Therefore, the values of sediment concentration, c , are not those required for the hydraulic simulation shown in [24] but should be larger. The sediment concentration, c , for computing the solid-liquid hydrograph of the Jaron di Sacomedan is assumed to be 0.45 for the MPD scenario. This is because the limited supply of sediments upstream of the enlargement does not allow the entrainment of large quantities of sediment, and the reach between the enlargement and the deposition area is short. For the MV scenario, the of c is diminished to 0.3. The value of the sediment concentration used for computing the solid-liquid hydrograph for the MPD scenario in the Jaron dei Ross basin is estimated using the sediment volume derived by the power-law relationship of [43], $V_{SED} = 77,000 A_B^{1.01}$, where A_B (km^2) is the area of the basin corresponding to the fan apex. This relationship was determined by a statistical distribution of data from debris flows that occurred, and the coefficient and exponent vary with the percentile. The relationship used in the present work corresponds to the 99th percentile due to the large quantity of

sediment lying on the upper part of the Jaron dei Ross basin. The value of A_B for the Jaron dei Ross basin is 0.67 km^2 , yielding $V_{SED} = 51,500 \text{ m}^3$. The volume of the debris flow is the sum of the runoff volume contributing to the debris flow and the sediment volume (under design conditions, the eroded volume is considered saturated). The sediment concentration is the ratio between the solid volume V_S ($V_S = c_* V_{SED}$) and the solid-liquid volume V_{SL} . The runoff contributing to debris flow is the sum of the corresponding volumes from Catchments 1–2 that supply the debris flow descending along the DF channel 1. For debris flow descending along DF channels 2–4, the runoff contributing to debris flow is the sum from Catchments 2–4, which is smaller than the previous case (Figure 9). Therefore, the previous case represents the design condition. The sediment concentration for the MPD scenario is 0.55, smaller than the maximum possible value of 0.66 ($0.9c_*$) according to [23]. For the MV scenario, the sediment concentration is smaller than that for the MPD scenario and is assumed to be 0.4. By using the adopted values of c , the solid-liquid hydrographs are computed by means of Equation (2) and shown in Figure 10. The sediment volume that can be deposited is that entrained during the downstream routing, that corresponding to solid-liquid hydrographs with c , according to Table 2. It is estimated by dividing the solid volume, cV_{SL} , by the sediment concentration at deposition, assumed equal to 0.62 according to [39] (it is smaller than the rest sediment concentration of the debris material in the upper part of the basin that is more compacted). Finally, the liquid flow from Catchments 1, 3 and 4 in the absence of debris flow can entrain a large volume of sediment that should be considered in pre-sizing computations. Therefore, we assume sediment concentration values of 0.3 and 0.2 for the MPD and MV scenarios respectively. In such cases, the solid-liquid volume is computed using Equation (2) with the whole runoff volume instead of the contributing volume to debris flow V_{CR} because the transport process is an high-intensity sediment transport. The sediment volume corresponding to the MPD scenario for the Jaron di Sacomedan basin, Jaron dei Ross basin, and Catchments 3 and 4 is 15,000, 51,500, and 6000 m^3 , respectively, whereas for the MV scenario, it is 40,000, 73,000 and 11,000 m^3 , respectively. Conversely, the values of the sediment concentration used for the hydraulic modeling are smaller. They are shown together with those for pre-sizing in Table 2. For the MPD scenario, the value of c for the Jaron di Sacomedan basin is assumed to be 0.3, while for the Jaron dei Ross is 0.4. The former is due to the limited sediment supply upstream of input section, while the latter is about 75% of the pre-sizing value, a reasonable value so that the sediment concentration of debris flow reaches the value corresponding to the relationship provided by [41] at the apex of the fan. The sediment concentrations for the MV scenario are half of those for the MPD scenario. The input solid-liquid hydrographs for the hydraulic simulations are those shown in Figure 10, but they are scaled with the ratio between the c values corresponding to the hydraulic simulation and pre-sizing.

Table 2. Values of the sediment concentration of the input hydrographs of both the scenarios used for the pre-sizing and for the hydraulic simulations.

Basin	Pre-Sizing		Hydraulic Simulations	
	MPD	MV	MPD	MV
Jaron di Sacomedan channel	0.45	0.3	0.3	0.15
Jaron dei Ross channel 1	0.55	0.4	0.4	0.3
Catchments 1, 3, 4	0.3	0.2	-	-

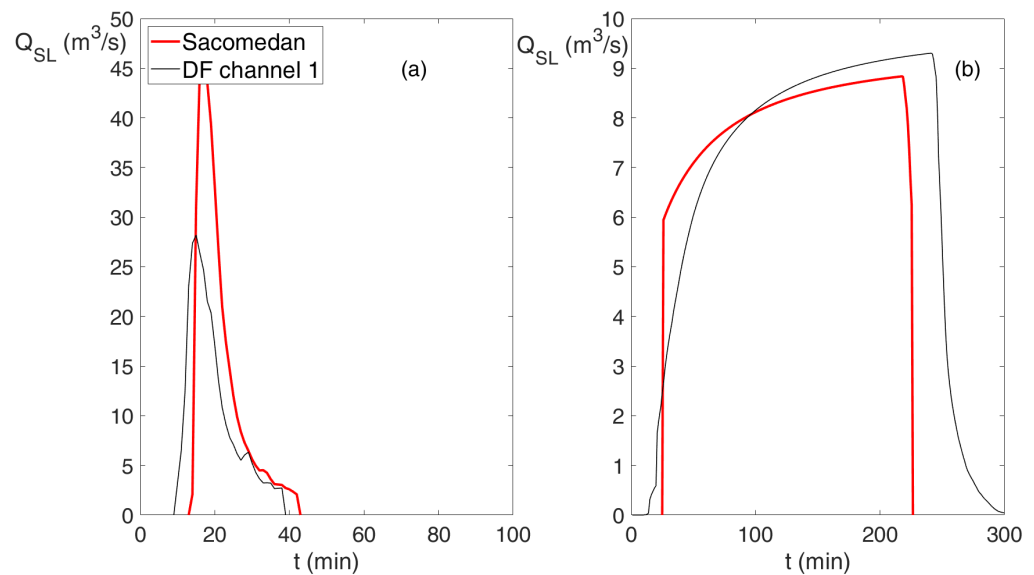


Figure 10. Computed solid-liquid hydrographs of the Jaron di Sacomedan basin and Catchment 2 of the Jaron dei Ross basin corresponding to the MPD (a) and MV (b).

3.2. Control Works on the Upper Part of Jaron Dei Ross Basin

The debris-flow channel was dammed by a wall, diverting the flow along DF channel 1 (Figure 3). Over the years, this solution failed because the wall was first subjected to piping, and then, in 2018, it partially failed due to the impact of a debris flow originating at the foot of the cliffs, while DF channel 1 was interrupted by a rockslide below its head. Finally, the rockfall of 2021 also determined the failure of the remaining part of the wall. All these events lead to the reactivation of the old debris-flow channel. Therefore, a new solution needs to be approached. This is the starting point for control works in the upper part of the Jaron dei Ross basin. The solution to the ephemeral channels that form at the base of the cliffs and incise the upper part of the scree involves the construction of an intake to divert the possible flow from the ephemeral channels to DF channel 1 (Figure 11). This also includes separating the intake-head of DF channel 1 from the active channel by constructing a bank supported by four mechanically stabilized earth retaining walls, built using the debris material in situ (Figure 11a). In this way, any ephemeral channels forming on the upper part of the scree of the Jaron dei Ross and converging toward the old wall position are drained by DF channel 1, with the subsurface flow being drained by the material composing the retaining walls. If the debris material from a rock failure covers the ephemeral channels, the flow is still intercepted by the intake and diverted to DF channel 1. If the debris material from a rock failure interrupts DF channel 1, the flow overtops the bank supported by the retaining walls and is conveyed along the old DF channel of Jaron dei Ross. Considering the potential occurrence of debris-flow events before the restoration of DF channel 1, three DF channels (2–4, shown in Figure 2) are built to divert the flow to a new deposition area. The number of DF channels is redundant to account for the possibility of multiple debris-flow events or rock failures that can block them. DF channels 2–4 are designed to each convey a 300-year return event, that is, the peak discharge of Figure 10, which also ensures a freeboard of 1.5 m.

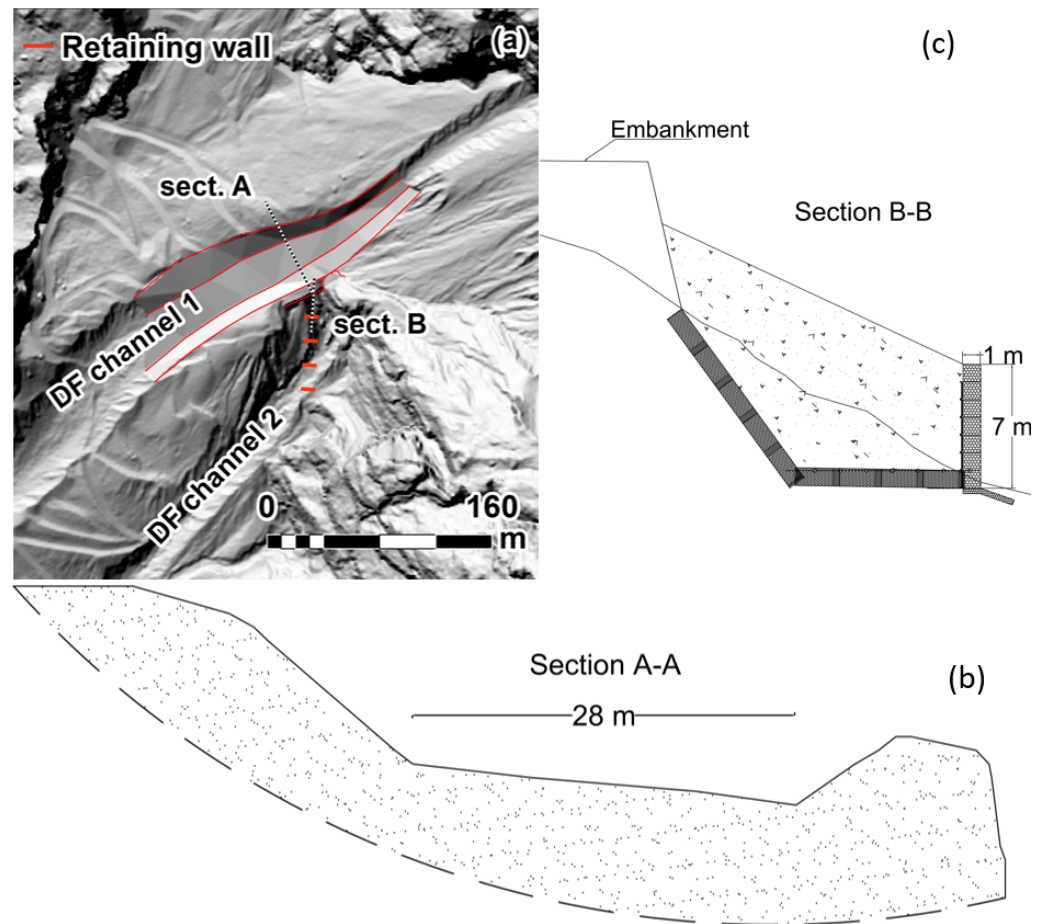


Figure 11. Plan view of control works in the upper part of the Jaron dei Ross scree with the red lines delimiting the new channel, (a) together with the cross and longitudinal sections of DF channel 1 (b) and the mechanically stabilized earth-retaining wall (c).

3.3. Control Works on the Lower Part of Jaron Di Sacomedan and Jaron Dei Ross Basins

The existing deposition area is extended upstream to enlarge it and to better intercept DF channels 1–3. Because the lower ends of the Jaron di Sacomedan and DF channels 1–4 are at different elevations, the deposition area is composed of two flat parts separated by a sloping section inclined at 20° (Figure 12). The sloping part also serves to direct the flow along the longitudinal direction for a better filling of the lower flat part of the deposition area. The deposition area is sized using the three-step procedure proposed in [23] and outlined in Deposition Area: Scope, Use, and Sizing Section. The initial or pre-sizing value of the area is determined using Equation (7). The deposition volume is the sum of the sediment volumes transported by debris flows along the channels of Sacomedan and DF 1: $40,000 + 73,000 + 11,000 \text{ m}^3$. The largest value of this sum corresponds to the MV scenario and is $124,000 \text{ m}^3$. It yields

$$A = \left(\frac{V}{k_D} \right)^{2/3} = \left(\frac{123,000}{0.1} \right)^{2/3} = 13,900 \text{ m}^2 \quad (10)$$

By using the initial value of $A = 13,900 \text{ m}^2$, we used GIS to design the deposition area with a value of $A \approx 16,000 \text{ m}^2$ (Figure 12). This value of A is much larger than the initial one because the deposition area intercepts up to five debris-flow channels, resulting in non-uniform deposition in the area due to preferential flow paths so that the deposition surface has a smaller inclination, and therefore the deposition volume is also smaller [23]. The sediment volume that can be stored is computed using Equation (8) with $\varphi_1 = 11^\circ$ for considering the non-uniform deposition instead of $\varphi_1 = 15^\circ$. The result is $132,000 \text{ m}^3$, and

the deposition area can store all the sediment volume arriving from the Sacomedan and DF channels 1–3. In the case of DF channel 4, it can only partially store the sediment volume of a debris flow routing along DF channel 4. In this last scenario, the sediment volume that does not deposit on the lower flat part of the deposition area is trapped by the retention basin where the channel starting from the downstream border of the deposition area ends.

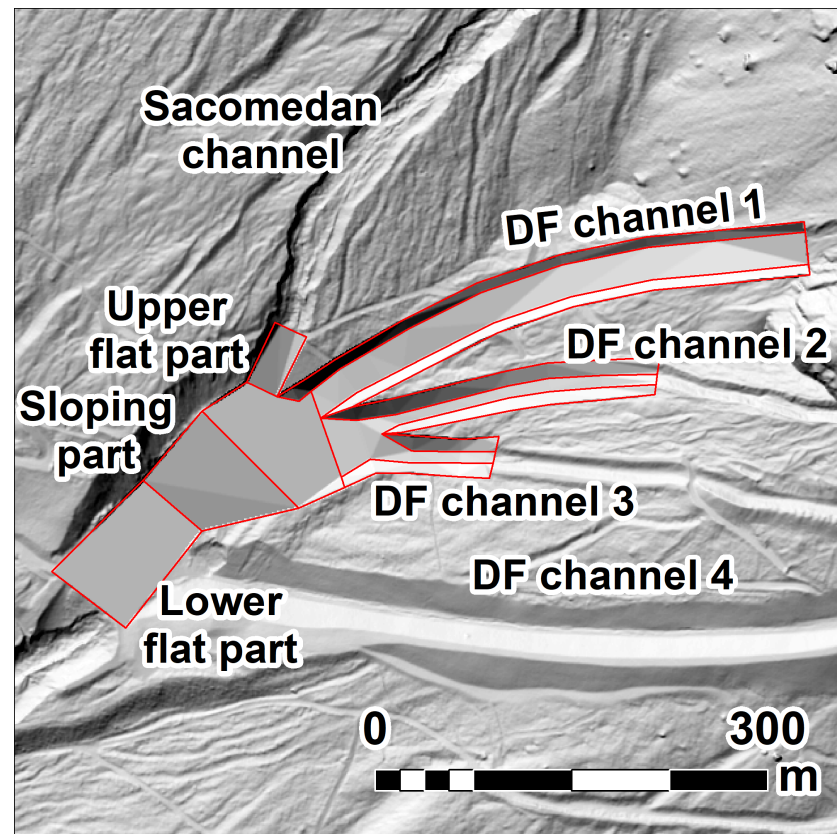


Figure 12. The new deposition area that intercepts the Sacomedan and the DF channels 1–4.

3.4. Analysis of the Proposed Solution, Its Sizing and Check

The proposed solution starts on the upper part of the Jaron dei Ross basin, where the debris flows from ephemeral channels are collected by a diversion channel and conveyed to a deposition area for the detention of the transported sediment volume. The potential occurrence of large rock failures and scree slides that interrupt the diversion channel is considered by building three other diversion channels for directing the debris flow to the deposition area. The other channels also provide safety during the restoration works after the occurrence of debris-flow events that fill DF channel 1 with sediment. The proposed solution shows the following advantages: (1) it is driven by the morphology of the terrain and avoids the building of concrete structures; (2) the channels are excavated on the fan, and the excavated debris is used to raise the downstream bank of each channel, imposing equality between terrain digging and filling; (3) the easy adjustment of the excavated works after observing debris-flow behavior; (4) the use of debris material, after an in-situ sieving for having uniform material, for building the mechanically stabilized earth retaining walls: respect to a concrete structure this dramatically reduces the costs and timing for its building, as well as those corresponding to the maintenance efforts; (5) the presence of DF channels 2–4 channelizes the debris flow along fixed path if the damming of DF channel 1 causes an avulsion, therefore avoiding uncontrolled and undesired flow paths [44,45]. The disadvantages include the maintenance of the efficiency of DF channels 1–4, by periodic surveys and possible restoration works after local rock and slope failures from the upstream side.

The use of the same deposition area for collecting the sediment volume of debris flows from two different basins represents an opportunity in terms of the proposed solution. The threats are limited because of the use of more diversion channels and the large size of the deposition area; the detention volume is a bit larger than the estimated sediment volume transported by the two debris flows (132,000 vs. 124,000 m³), and the same detention volume was computed using the smallest value of ϕ_1 , so that there is a reserve for storing a large value of sediment volume. When the deposition area is filled, a temporary early warning system can be installed to protect the road. Finally, the adopted method for sizing the channels and the deposition area using the sediment volume of the solid-liquid hydrographs provides a consistent reduction of the design timing with respect to the use of hydraulic simulations, ensuring a satisfactory degree of reliability because of the adopted values of the sediment concentration. This is, somehow, confirmed by the hydraulic modeling corresponding to the two scenarios. Here, for the sake of simplicity, we show the two cases of input solid-liquid and liquid flows to DF channel 1 (liquid hydrograph from Catchment 1 and solid-liquid hydrograph from Catchment 2) and DF channel 2 (liquid hydrographs from Catchments 3 and 4) respectively, and liquid input to DF channel 1 (liquid hydrograph from Catchment 1) and solid-liquid and liquid inputs to DF channel 2 (solid-liquid hydrograph from Catchment 2 and liquid hydrographs from Catchments 3 and 4), respectively. The routing of solid-liquid and liquid flows along DF channel 3 is, in fact, similar to that along DF channel 2. The solid-liquid flow routing along DF channel 4 does lead to a partial filling of the two deposition areas, so this case does not represent the more costly conditions for the works in the upper part of the basin. Figures 13 and 14 show the results of the hydraulic modeling for the two cases and both the scenarios: the maximum flow depth and the erosion-deposition depth, respectively. In all the simulations, the flow is inside of the channel, and the freeboard is ensured.

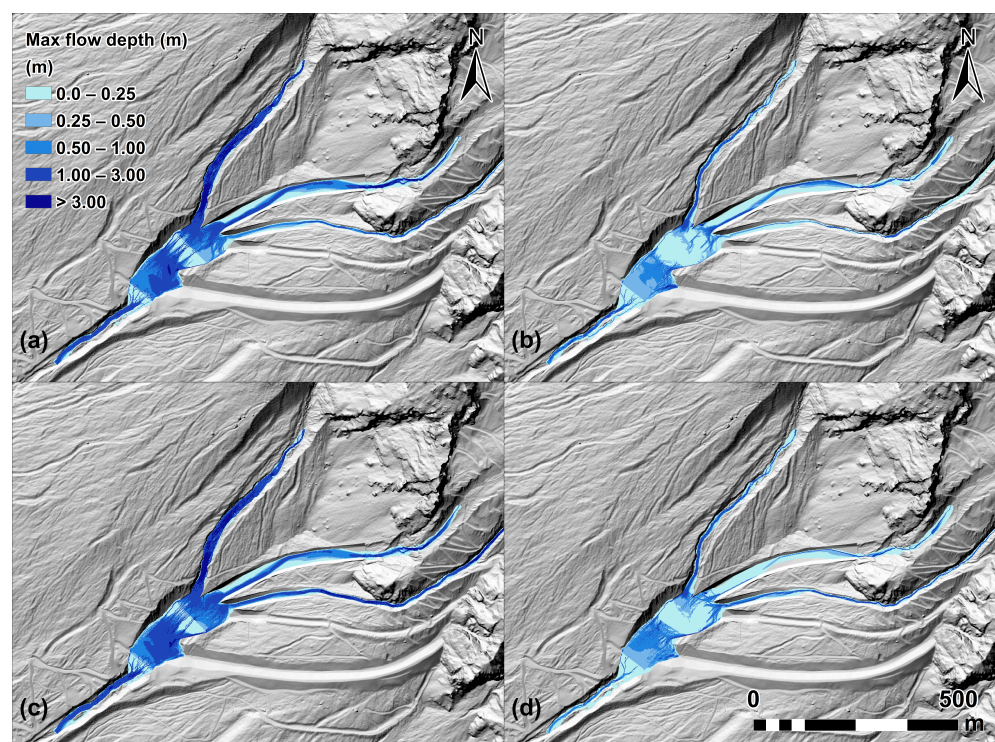


Figure 13. The results of hydraulic modeling in terms of maximum flow depth. The case of a solid-liquid input into the Sacomedan channel, solid-liquid and liquid inputs into DF channel 1, and liquid input into DF channel 2 for the MPD (a) and MV (b) scenarios, respectively; the case of solid-liquid input into the Sacomedan channel, liquid input into DF channel 1, and solid-liquid and liquid inputs into DF channel 2 for the MV (c) and MV (d) scenarios, respectively.

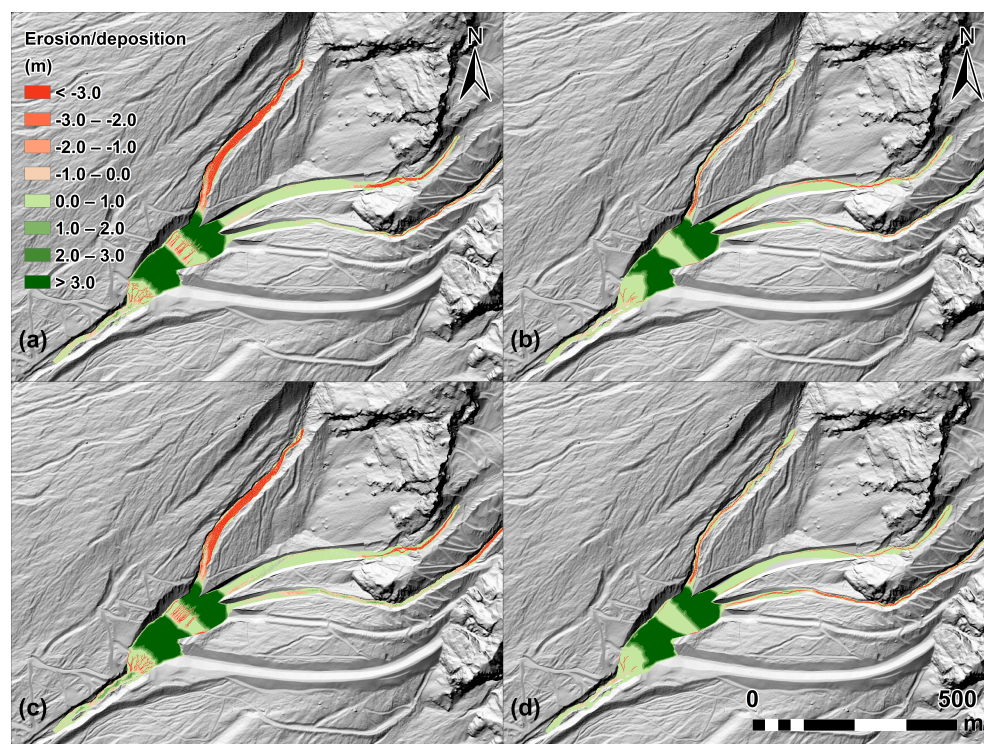


Figure 14. The results of hydraulic modeling in terms of deposition and erosion depths. The case of solid-liquid input into the Sacomedan channel, solid-liquid and liquid inputs into DF channel 1, and liquid input into DF channel 2 for the MPD (a) and MV (b) scenarios, respectively; the case of solid-liquid input into the Sacomedan channel, liquid input into DF channel 1, and solid-liquid and liquid inputs into DF channel 2 for the MV (c) and MV (d) scenarios, respectively.

The results of the sediment volumes entrained along channels and deposited in the deposition areas are shown in Table 3, together with the corresponding estimated and design values. The estimated values are those corresponding to the product $cV_{SL}/0.62$ with V_{SL} computed using Equation (2) and c according to Table 2. The design value is the deposition volume corresponding to the designed area. The simulated deposition volumes for both scenarios are smaller than the design value, with those of the MPD scenario smaller than those of MV scenario. The largest value of the simulated deposition volume is $106,000 \text{ m}^3$ (MV scenario and input-solid flow to DF channel 1), which is about 20% smaller than the design value of $132,000 \text{ m}^3$. This confirms the sizing of the deposition area and also shows the availability of a reserve volume for stopping debris material transported by following events of debris-flow occurring before the emptying of the deposition area. The lower values of the simulated deposition volume with respect to the sizing version are explained by the outflow from the deposition area. The hydraulic simulations, on the other side also show that the estimated sediment volume entrained on the single channels by means of the pre-sizing values of sediment concentration in Table 2 are different from those simulated. In particular, for the MPD scenario, the sediment volume entrained on the Jaron di Sacomedan channel is much larger (more than 100 %) than the estimated value, whereas that on the Jaron dei Ross DF channels 1 and 2 is much smaller (about the 50%). The sediment volume entrained on DF channels 1 and 2 when stressed by an input liquid flow is also much larger than the estimated volume. A reason for this discrepancy, could be the very large value of the input-solid liquid discharge to the Jaron di Sacomedan channel: the entrainment is, in fact, somehow proportional to the value of the input discharge according to [32,40]. For the MV scenario the sediment volume entrained in all the channels stressed by an input solid-liquid flow is about 15–25 % smaller than the estimated volume. The simulated deposition volume is smaller for the case of solid-liquid input into the Jaron dei Ross DF channel 1 for both scenarios. Finally, Table 3 also shows that the sum of

the entrained sediment volume is larger than that deposited on the deposition area for both scenarios. The net difference provides useful information about the sizing of the downstream retention basin.

Table 3. Comparison between the sizing and simulated values of the sediment volumes (m³) trapped in the deposition area for both scenarios.

Scenario of the Maximum Debris-Flow Peak Discharge				
solid-liquid inputs to Sacomedan channel and DF channel 1				
Zone	net entrained volume	estimated volume	net deposited volume	design volume
Sacomedan channel	53,500	15,000	-	-
DF channel 1	32,500	51,500	-	-
DF channel 2	8900	6000	-	-
Deposition area	-	-	87,000	132,000
solid-liquid inputs to Sacomedan channel and DF channel 2				
Zone	net entrained volume	estimated volume	net deposited volume	design volume
Sacomedan channel	51,600	15,000	-	-
DF channel 1	25,300	6000	-	-
DF channel 2	27,500	51,500	-	-
Deposition area	-	-	93,300	132,000
Scenario of the Maximum Debris-Flow Volume				
solid-liquid inputs to Sacomedan channel and DF channel 1				
Zone	net entrained volume	estimated volume	net deposited volume	design volume
Sacomedan channel	31,900	40,000	-	-
DF channel 1	59,900	73,000	-	-
DF channel 2	9600	11,000	-	-
Deposition area	-	-	81,700	132,000
solid-liquid inputs to Sacomedan channel and DF channel 2				
Zone	net entrained volume	estimated volume	net deposited volume	design volume
Sacomedan channel	29,600	40,000	-	-
DF channel 1	19,100	11,000	-	-
DF channel 2	66,600	73,000	-	-
Deposition area	-	-	106,100	132,000

4. Discussion

Traditional control works typically intercept debris flows along their path and store the sediment volume. However, in this case, it is not feasible, and the flow must be diverted into a channel that guides it toward an area where the sediment can be stored. The present case is unique because the head of the diversion channel cuts through a scree at the base of rocky cliffs that are frequently subject to failures. The falling debris alters the morphology of the scree, causing debris-flow channels that form at the base of the cliffs after intense precipitation to become ephemeral as they are eventually covered by the failed material. A more permanent debris-flow channel forms further downstream, where the subsurface flow from the large part of the scree converges, as shown by the electrical tomography. This explains the failure of the solution adopted in 1980: a wall damming the head of the debris-flow channel was subjected to piping and failed twice. To overcome this issue, an embankment supported by four mechanically stabilized earth-retaining walls is constructed to block the channel and form the left bank of the diversion channel (DF channel 1 in Figure 2). The embankment and retaining walls are made of debris material, allowing for easy drainage of subsurface flow. In addition, an intake is built upstream of the embankment to drain any ephemeral channels that may form at the base of the

cliff. In the event of a large cliff failure filling the diversion channel, three other diversion channels (DF channels 2–4 in Figure 2) are constructed downstream of the retaining walls. All these diversion channels direct the flow to a deposition area designed to also collect the debris flow from the Jaron di Sacomedan basin. The deposition area consists of two flat parts separated by a sloping section, as the mouths of all channels (DF channels 1–4 and the Sacomedan one) are at different elevations. The sizing of this area follows the framework proposed in [24], which has been updated to estimate the sediment volume transported by debris flows without requiring hydraulic simulations of debris-flow routing. The sizing value of the deposition volume for the deposition area exceeds the simulated values because there is always an outflow from the deposition area. This provides a reserve volume for the detention of further sediments transported by following events before the end of the restoration works. The hydraulic simulations show that the estimated entrained sediment volume on debris-flow channels in the MPD scenario is much different from the sizing value. This is explained by the influence of the input discharge values and morphology. Essentially, this work demonstrates the planning and sizing of control works in a site with dynamic morphology where previous attempts failed. The proposed solution adapts to the changing landscape and provides an update to the framework in [24] for sizing the works without carrying out preliminary hydraulic simulations.

5. Conclusions

Usual works for controlling debris flow are positioned in the medium and lower parts of a basin where slopes are gentler and their construction, as well as the maintenance activity, is facilitated. In the case of the Jaron dei Ross basin, this is not possible because of the lack of space for the detention of the sediment volume transported by debris flows. Therefore, the debris flow must be redirected to another place where the construction of a detention basin is suitable. The morphological variability of the upper part of the Jaron dei Ross basin for which ephemeral debris-flow channels can originate and end leads to the solution of a main debris-flow channel that can intercept all of them and convey the debris flow to a suitable location where a deposition area can store the transported sediment volume. Safety requirements mandate the construction of three other debris-flow channels for the redirection of debris flow to prevent the case of the filling of the main diversion channel with deposits of sediment from slide or from the stopping of small-magnitude and inertia debris-flow events. In addition, the location of the deposition area was chosen to collect debris flow from the neighboring basin of Jaron di Sacomedan, therefore concentrating both the control works and restoration activities within a unique point. Finally, a pre-existing framework for the sizing of the control works is updated to speed up the sizing procedure in such a complex situation.

Author Contributions: Conceptualization, M.B. (Martino Bernard), M.B. (Mauro Boreggio) and C.G.; methodology, M.B. (Martino Bernard), M.B. (Mauro Boreggio) and C.G.; software, M.B. (Matteo Barbini); validation, M.B. (Martino Bernard), M.B. (Mauro Boreggio) and C.G.; formal analysis, M.B. (Martino Bernard); investigation, M.D.; resources, C.G.; data curation, M.B. (Mauro Boreggio); writing—original draft preparation, M.B. (Mauro Boreggio); writing—review and editing, M.B. (Martino Bernard); M.B. (Mauro Boreggio); C.G.; project administration, M.B. (Mauro Boreggio); funding acquisition, C.G. All authors have read and agreed to the published version of the manuscript.

Funding: This work was supported by the following funds: European Union Next Generation EU, National Recovery, and Resilience Plan—NRRP, Mission 4, Component 2, Investment 1.3—D.D. 1243 2/8/2022, PE0000005 (RETURN Extended Partnership); Fondazione Cassa di Risparmio di Padova e Rovigo (Excellence Grant 2021 to the RESILIENCE Project “extreme storms in the Italian North-East: frequency, impacts and projected changes”); Università degli Studi di Padova (grants numbers DOR2330507/23) “Use of the deposition areas for the reduction of the sediment volume transported by debris flows” and BIRD2024 “Model-based Early Warning System for the Prediction of Debris-flow Occurrence and Magnitudo”.

Data Availability Statement: The original contributions presented in the study are included in the article, further inquiries can be directed to the corresponding author.

Acknowledgments: Main part of this work was commissioned by the Soil Defence and Civil Protection Department of the Province of Belluno that also provided the LiDAR data from 2011; Veneto Region supplied the LiDAR data from 2015 and 2021. The authors wish to thank Diego Albanese, Giuseppe Frescura, and Laura Paludetti for their assistance with the electrical tomography; Simonetta Cola for her help with the triaxial test. A final thank to the personnel of the Province of Belluno—K. Biasuzzi, L. Soppelsa, and R. Mezzomo—for the help provided during the work.

Conflicts of Interest: The authors declare no conflicts of interest.

Abbreviations

The following abbreviations are used in this manuscript:

DEM	Digital Elevation Model
LiDAR	Light Detection and Ranging
MDP	Maximum Peak Discharge
MV	Maximum Volume

Appendix A. Depth Frequency Curve

The sampling of annual maximum events is a simple methodology to apply and ensures the fulfillment of conditions of independence and the identical distribution of events, but it is limited, as it considers only one value for each time block. In doing so, there is a possibility that very intense precipitation events with precipitation heights lower than the annual maximum value but higher than the annual maximum values observed in other years may be excluded from the analysis. To avoid this, the Peaks Over Threshold (POT) technique was developed [41]. The fundamental idea behind this method is to analyze the extremes of a quantity X based on exceedances, that is, when given a set of data (x_1, x_2, \dots, x_n) , consider those values, x_i , to be greater than a threshold value, x_0 . The quantity $y_i = x_i - x_0$ is called the exceedance, value, or excess above the threshold.

The analysis involves fitting two distributions: the first determines the number of events in the observed time period, and the second is used for exceedances. When the number of observations tends to infinity, the distribution of the number of events above the threshold, assuming they are uncorrelated and independent, approximates a Poisson distribution:

$$p(m) = \frac{\lambda^m}{m!} e^{-\lambda} \quad (\text{A1})$$

where m is the number of events above the threshold, and λ is the ratio between the number of exceedances m and the number of observed years N . At the same time, it can be assumed that the distribution of exceedances follows a Generalized Pareto (GP) distribution:

$$G(y) = 1 - \left(1 + \xi \frac{y}{\sigma}\right)^{-1/\xi} \quad (\text{A2})$$

where ξ is the shape parameter, and σ is the scale parameter of the distribution, which are to be calibrated by fitting the distribution to the observed exceedances y . The parameters ξ and σ were estimated using the method of linear moments or L-Moments [46]. This method was chosen because linear moments are calculated as a linear function of the sample data and are almost unbiased for all probability distributions and for small sample sizes [47]. The expressions for the linear moments are

$$l_1 = b_0, l_2 = 2b_1 - b_0 \quad (\text{A3})$$

$$b_r = m^{-1} \binom{m-1}{r}^{-1} \sum_{j=r+1}^m \binom{j-1}{r} x_{j:m} \quad (\text{A4})$$

from which we derive the parameters of the GP distribution:

$$\xi = \frac{x_0 - l_1 + 2l_2}{l_2}, \sigma = l_2(1 - \xi)(2 - \xi) \quad (\text{A5})$$

Once the distributions are calibrated on the sample, it is possible to calculate the precipitation, h , related to the design return period, T_R , as

$$h(T_R) = x_0 + \frac{\sigma}{\xi} \left(\frac{1}{\lambda T_R}^{-\xi} - 1 \right) \quad (\text{A6})$$

In this approach, the choice of the threshold value x_0 becomes fundamental. It must be sufficiently high to allow compliance with the assumptions of extreme value theory but also to allow for the creation of a sufficiently large and statistically significant sample.

Appendix B

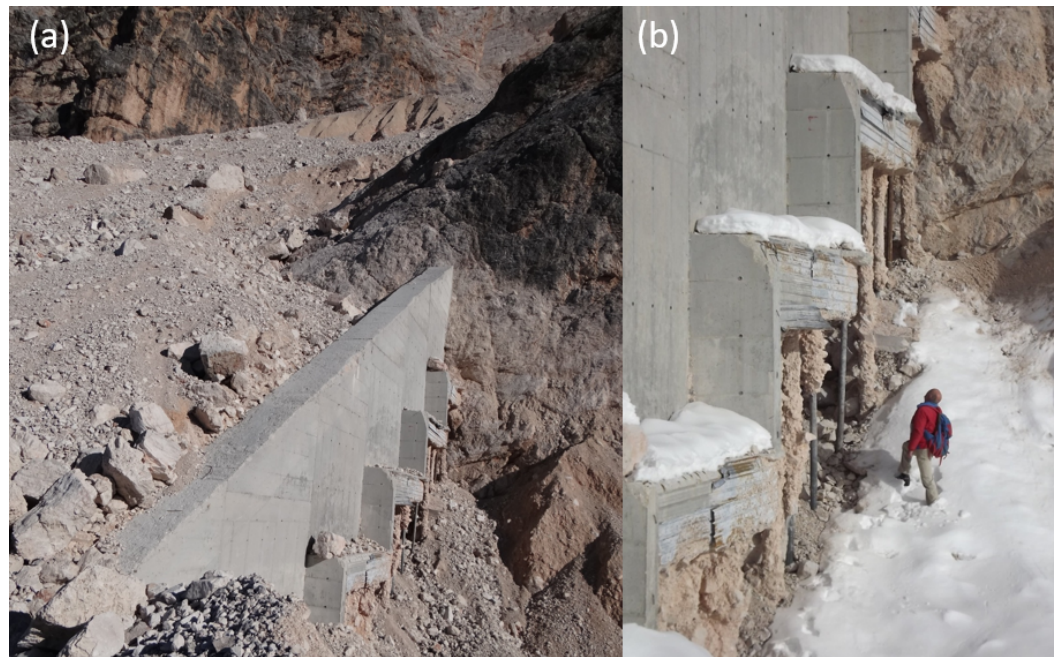


Figure A1. A general view (a) of the wall subjected to piping with the particular of foundation (b). The images were taken on 2012 (courtesy of R. Mezzomo).

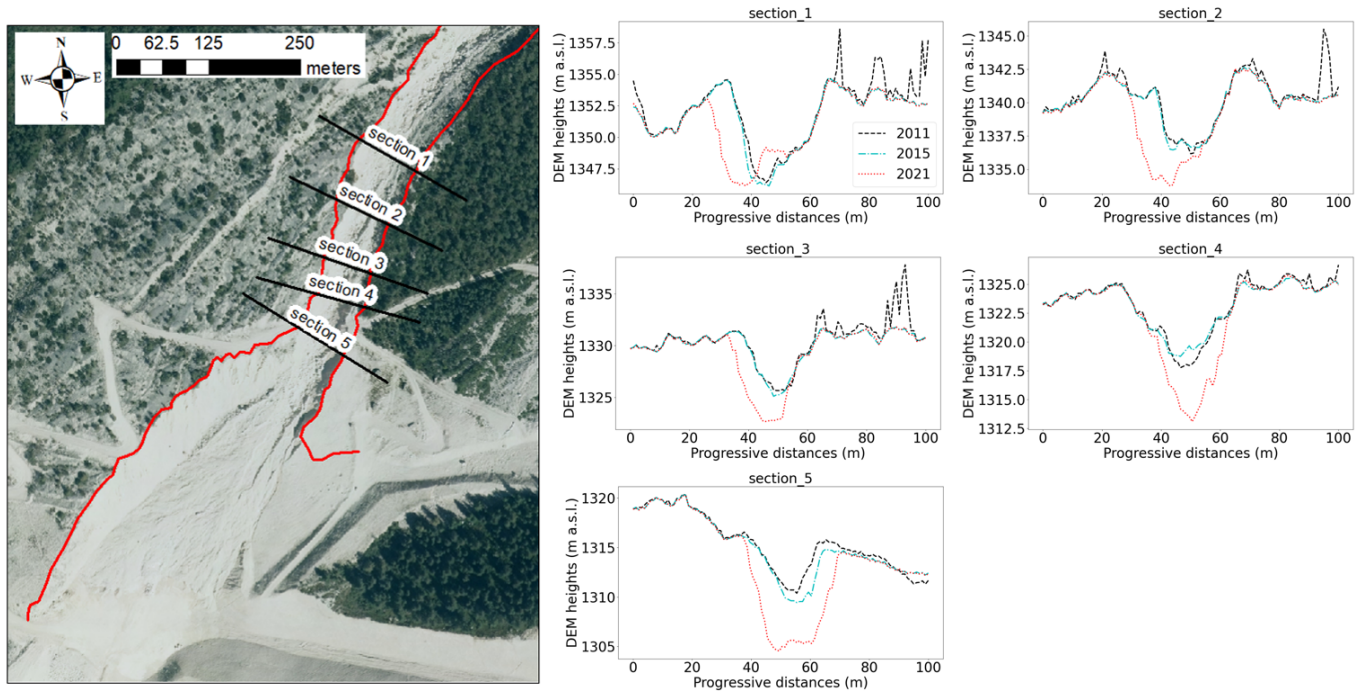


Figure A2. Areal view of the mouth of the Sacomedan channel (left) with the in-time variations of the cross-sections.

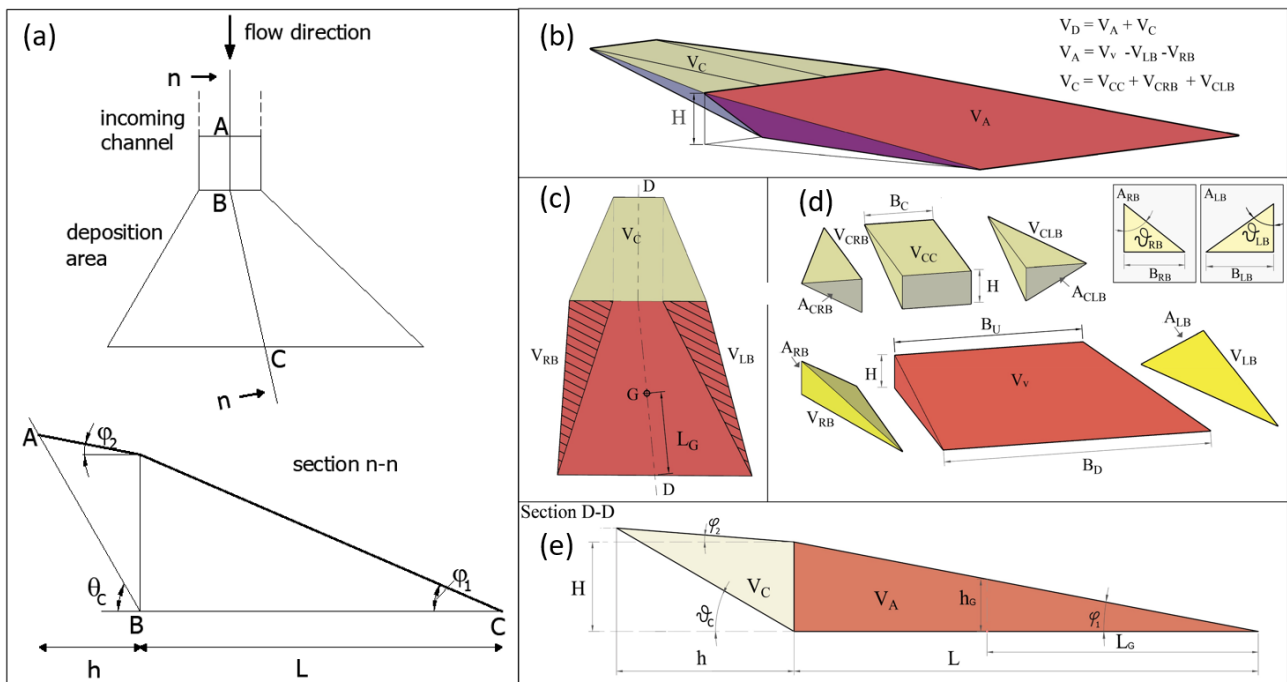


Figure A3. Deposition volume: schematic plan and profile views (a); detailed 3D (b,d); plan (c) views and the vertical section along the longitudinal axis (e) (modified and redrawn from [23]).

References

1. Berti, M.; Genevois, R.; LaHusen, H.; Simoni, A.; Tecca, P.R. Field observations of a debris flow event in the Dolomites. *Geomorphology* **1999**, *29*, 265–274. [CrossRef]
2. Berti, M.; Simoni, A. Experimental evidences and numerical modelling of debris flow initiated by channel runoff. *Landslide* **2005**, *2*, 171–182. [CrossRef]
3. Imaizumi F.; Sidle, R.C.; Tsuchiya, S.; Ohsaka, O. Hydrogeomorphic processes in a steep debris flow initiation zone. *Geophys. Res. Lett.* **2006**, *33*, L10404. [CrossRef]

4. Coe, J.A.; Kinner, D.A.; Godt, J.W. Initiation conditions for debris flows generated by runoff at Chalk Cliffs, central Colorado. *Geomorphology* **2008**, *96*, 270–297. [[CrossRef](#)]
5. Kean, J.W.; McCoy, S.W.; Tucker, G.E.; Staley, D.M.; Coe, J.A. Runoff-generated debris flows: Observations and modeling of surge initiation, magnitude and frequency. *J. Geophys. Res.* **2013**, *118*, 2190–2207. [[CrossRef](#)]
6. Theule, J.I.; Liebault, F.; Loye, A.; Laigle, D.; Jaboyedoff, M. Sediment budget monitoring of debris flow and bedload transport in the Manival Torrent, SE France. *Nat. Hazard Earth Sci.* **2012**, *12*, 731–749. [[CrossRef](#)]
7. Theule, J.; Liébault, F.; Laigle, D.; Loye, A.; Jaboyedoff, M. Channel scour and fill by debris flows and bedload transport. *Geomorphology* **2015**, *243*, 92–105. [[CrossRef](#)]
8. Reid, M.E.; Coe, J.A.; Dianne, L.B. Forecasting inundation from debris flows that grow volumetrically during travel, with application to the Oregon Coast Range, USA. *Geomorphology* **2016**, *273*, 396–411. [[CrossRef](#)]
9. Simoni, A.; Bernard, M.; Berti, M.; Boreggio, M.; Lanzoni, S.; Stancanelli, M.L.; Gregoretti, C. The title of the cited article. *Earth Surf. Process Landf.* **2020**, *45*, 3556–3571. [[CrossRef](#)]
10. Rengers, F.K.; McGuire, L.A.; JW Kean, J.W.; Staley, D.M.; Dobre, M.; Swetnam, T. Movement of sediment through a burned landscape: Sediment volume observations and model comparisons in the San Gabriel mountains, California, USA. *J. Geophys. Res.-Earth Surf.* **2021**, *126*, e20209JF006053. [[CrossRef](#)]
11. Fannin, R.J.; Wise, M.P. An empirical–statistical model for debris flow travel distance. *Can. Geotech. J.* **2001**, *38*, 982–994. [[CrossRef](#)]
12. Bollschweiler, M.; Stoffel, M. Changes and trends in debris-flow frequency since AD 1850: Results from the Swiss Alps. *Holocene* **2021**, *20*, 907–916. [[CrossRef](#)]
13. Flores, J.; D’Alpaos, A.; Squarzoni, C.; Genevois, R.; Marani, M. Recent changes in rainfall characteristics and GIS and their influence on threshold for debris flow triggering on Dolomitic area of Cortina d’Ampezzo, North-eastern Italian Alps. *Nat. Hazard Earth Syst. Sci.* **2010**, *10*, 571–580. [[CrossRef](#)]
14. Damm, B.; Felder, A. Impact of atmospheric warming on permafrost degradation and debris flow initiation—A case study from the eastern European Alps. *EG Quat. Sci. J.* **2013**, *62*, 136–149. [[CrossRef](#)]
15. Stoffel, M.; Tiranti, D.; Huggel, C. Climate change impacts on mass movements—Case studies from the European Alps. *Sci. Total Environ.* **2014**, *493*, 1255–1266. [[CrossRef](#)] [[PubMed](#)]
16. Rengers, F.K.; Kean, J.W.; Reitman, N.G.; Smith, J.B.; Coe, J.A.; McGuire, L.A. The influence of frost weathering on debris flow sediment supply in an alpine basin. *J. Geophys. Res.-Earth Surf.* **2020**, *125*, e2019JF005369. [[CrossRef](#)]
17. Franceschinis, C.; Thiene, M.; Mattea, S.; Scarpa, R. Do information and citizens characteristics affect public acceptability of landslide protection measures? A latent class approach. *Clim. Change Manag.* **2020**, 503–513.
18. Musumeci, R.E.; Foti, E.; Rosi, D.L.; Sanfilippo, M.; Stancanelli, L.M.; Iuppa, C. Debris-flow hazard assessment at the archaeological unesco world heritage site of villa romana del casale (sicily, italy). *Int. J. Disaster Risk Reduct.* **2021**, *64*, 102509. [[CrossRef](#)]
19. Strouth, A.; McDougall, S. Societal risk evaluation for landslides: Historical synthesis and proposed tools. *Landslides* **2021**, *18*, 1071–1085. [[CrossRef](#)]
20. Piton, G.; Recking, A. Design of Sediment Traps with Open Check Dams. I: Hydraulic and Deposition Processes. *J. Hydraul. Eng.* **2016**, *142*, 04015045. [[CrossRef](#)]
21. Hübl, J. Conceptual framework for sediment management in torrents. *Water* **2018**, *110*, 1718. [[CrossRef](#)]
22. Johnson, P.A.; McCuen, R.H.; Hromadka, T.V. Debris basin policy and design. *J. Hydrol.* **1991**, *123*, 83–95. [[CrossRef](#)]
23. Bernard, M.; Barbini, M.; Boreggio, M.; Biasuzzi, K.; Gregoretti, C. Deposition areas: An effective solution for the reduction of the sediment volume transported by stony debris flows on the high-sloping reach of channels incising fans and debris cones. *Earth Surf. Process Landf.* **2024**, *49*, 664–683. [[CrossRef](#)]
24. Barbini, M.; Bernard, M.; Boreggio, M.; Schiavo, M.; Gregoretti, C. An alternative approach for the sediment control of in-channel stony debris flows with an application to the case study of the Ru Secco Creek (Venetian Dolomites, Northeast Italy). *Front. Earth Sci.* **2024**, *12*, 1340561. [[CrossRef](#)]
25. Piton, G.; D’Agostino, V.; Horiguchi, T.; Hübl, J. Functional design of mitigation measures: From design event definition to targeted process modifications. In *Advances in Debris-Flow Science and Practice*; Jakob, M., McDougall, S., Santi, P.M., Eds.; Springer: Berlin, Germany, 2024; pp. 495–538.
26. Giovannini, L.; Davolio, S.; Zaramella, M.; Zardi, D.; Borga, M. Multi-model convection-resolving simulations of the October 2018 Vaia storm over Northeastern Italy. *Atmos. Res.* **2021**, *253*, 105455. [[CrossRef](#)]
27. Bunte, K.; Abt, S.R. *Sampling Surface and Subsurface Particle-Size Distributions in Wadable Gravel-and Cobble-Bed Streams for Analyses in Sediment Transport, Hydraulics, and Streambed Monitoring*; General Technical Report RMRS-GTR-74; US Department of Agriculture, Forest Service, Rocky Mountain Research Station: Fort Collins, CO, USA, 2001.
28. Schiavo, M. Entropy, fractality, and thermodynamics of groundwater pathways. *J. Hydrol.* **2023**, *623*, 129824. [[CrossRef](#)]
29. Gregoretti, C.; Degetto, M.; Bernard, M.; Crucil, G.; Pimazzoni, A.; De Vido, G.; Berti, M.; Simoni, A.; Lanzoni, S. Runoff of small rocky headwater catchments Field observations and hydrological modeling. *Water Resour. Res.* **2016**, *52*, 8138–8158. [[CrossRef](#)]
30. Orlandini, S.; Rosso, R. Diffusion Wave Modeling of Distributed Catchment Dynamics. *J. Hydrol. Eng.* **1996**, *1*, 103–113. [[CrossRef](#)]
31. Bernard, M.; Barbini, M.; Berti, M.; Simoni, A.; Boreggio, M.; Gregoretti, C. Rainfall-Runoff Modelling in Rocky Headwater Catchments for the Prediction of Debris Flow Occurrence. *Water Resour. Res.* **2025**, *61*. [[CrossRef](#)]
32. Lanzoni, S.; Gregoretti, C.; Stancanelli, L.M. Coarse-grained debris flow dynamics on erodible beds. *J. Geophys. Res. Earth Surf.* **2017**, *122*, 592–614. [[CrossRef](#)]

33. Takahashi, T. *Debris Flows: Mechanics, Prediction and Countermeasures*; Taylor and Francis/Balkema: Leiden, The Netherlands, 2007.
34. Lien, P.H.; Tsai, F. Sediment concentration of debris flow. *J. Hydraul. Eng.* **2003**, *129*, 995–1000. [[CrossRef](#)]
35. Ferri, M.; Welber, M.; Facchini, M. The Computation of Solid-Liquid Hydrograph. em Private communication, 2003.
36. Gregoretti, C.; Fontana, G.D. The triggering of debris flow due to channel-bed failure in some alpine headwater basins of the Dolomites: Analyses of critical runoff. *Hydrol. Process.* **2008**, *22*, 2248–2263. [[CrossRef](#)]
37. Ma, C.; Deng, J.; Wang, R. Analysis of the triggering conditions and erosion of a runoff triggered debris flow in Miyun County, Beijing, China. *Landslide* **2018**, *15*, 2475–2485. [[CrossRef](#)]
38. Pastorello, R.; D'Agostino, V.; Hürlimann, M. Debris flow triggering characterization through a comparative analysis among different mountain catchments. *Catena* **2020**, *186*, 104348. [[CrossRef](#)]
39. Gregoretti, C.; Stancanelli, M.L.; Bernard, M.; Boreggio, M.; Degetto, M.; Lanzoni, S. Relevance of erosion processes when modelling in-channel gravel debris flows for efficient hazard assessment. *J. Hydrol.* **2019**, *569*, 575–591. [[CrossRef](#)]
40. Tognacca, C. Beitrag zur Untersuchung der Entstehungsmechanismen von Murgängen. Doctoral Thesis, ETH Zurich, Zurich, Switzerland, 1999.
41. Pickands, J., III. Statistical Inference Using Extreme Order Statistics. *Ann. Stat.* **1975**, *3*, 119–131.
42. Davison, A.C.; Smith, R.L. Models for Exceedances Over High Thresholds. *J. R. Stat. Soc. Ser. (Methodol.)* **1990**, *52*, 393–425. [[CrossRef](#)]
43. Marchi, L.; Brunetti, M.T.; Cavalli, M.; Crema, S. Debris-flow volumes in Northeastern Italy: Relationship with drainage and size probability. *Earth Surf. Landforms* **2019**, *44*, 933–943. [[CrossRef](#)]
44. Zubrycky, S.; Mitchell, A.; McDougall, S.; Strouth, A.; Clague, J.J.; Menounos, B. Exploring new methods to analyse spatial impact distributions on debris-flow fans using data from southwestern British Columbia. *Earth Surf. Process. Landforms* **2021**, *46*, 2395–2413. [[CrossRef](#)]
45. Schiavo, M.; Gregoretti, C.; Boreggio, M.; Barbini, M.; Bernard, M. Probabilistic identification of debris-flow pathways in mountain fans within a stochastic framework. *J. Geophys. Res. Earth Surf.* **2024**, *129*, e2024JF007946. [[CrossRef](#)]
46. Marra, F.; Nikolopoulos, E.I.; Anagnostou, E.N.; Morin, E. Metastatistical Extreme Value analysis of hourly rainfall from short records: Estimation of high quantiles and impact of measurement errors. *Adv. Water Resour.* **2018**, *117*, 27–39. [[CrossRef](#)]
47. Hosking, J.R.M. L-Moments: Analysis and Estimation of Distributions Using Linear Combinations of Order Statistics. *J. R. Stat. Soc. Ser. (Methodol.)* **1990**, *52*, 105–124. [[CrossRef](#)]

Disclaimer/Publisher's Note: The statements, opinions and data contained in all publications are solely those of the individual author(s) and contributor(s) and not of MDPI and/or the editor(s). MDPI and/or the editor(s) disclaim responsibility for any injury to people or property resulting from any ideas, methods, instructions or products referred to in the content.